Supplementary materials

S.1 Experimental Methods

S.1.1 Tissue Imaging

Live imaging of larvaceans. Four different larvacean species (*Bathochordaeus mcnutti, Bathochordaeus stygius, Fritillaria sp., Mesochordaeus erythrocephala*) were collected at water depths ranging from 55 m to 330 m in the Monterey Bay National Marine Sanctuary using acrylic detritus and suction samplers with remotely operated vehicles (ROVs) Ventana and Doc Ricketts as part of RVs Rachel Carson and Western Flyer cruises in May and October 2016, June 2018, and July 2021. Collected larvaceans were kept in seawater at 4°C for a maximum of 48 h before imaging analysis was conducted. For imaging, animals were placed in 10 cm petri dishes filled with seawater at 4°C that was regularly refreshed. The internal ciliated ducts were observed using phase contrast microscopy with 20x and 40x objectives. High-speed video microscopy was performed using either a Sony 4K Handycam FDR-AX700 or an SC1 camera (Edgertronic, CA, USA) mounted each with a custom optical adapter to the C-port or the eyepiece holder of the microscope. Ciliary beat frequency was measured from the videos using the kymograph plugin in ImageJ [1] which visualizes the number of beat cycles per second. Metachronal wave length and direction of propagation was derived from subsequent frames in high-speed video recordings as well as spacing and slope of the stripe pattern in kymographs. Flow was visualized by adding 1 to 10 μm sized glass microspheres microspheres (Dantec Dynamics, NY, USA) and 1 to 2 μm polymer microspheres (Cospheric, CA, USA) as tracer particles to the seawater. Fluid flow velocity magnitudes were measured from particle trajectories using the Trackmate plugin in ImageJ [2]. As the high density of cilia in the larvacean ciliated duct obscured the direct imaging of tracer particles, or prevented their passage, the fluid velocity magnitude within the duct was estimated from the flux in the funnel just outside the duct.

Immunofluorescence (IF) imaging of larvaceans. Animals were fixed in 4 percent paraformaldehyde in seawater for 24 h at 4°C, then washed 3x for 10-30 min in phosphate-buffered saline (PBS) and stored in PBS at 4°C until IF staining. For IF staining, the samples were incubated with primary monoclonal antibodies against α-acetylated tubulin (to stain cilia; T6793, Sigma-Aldrich, MI, USA) in PBS for 24 h at room temperature, followed by 24 h of incubation in anti-mouse secondary antibody (Invitrogen, CA, USA), phalloidin (to stain F-actin), and DAPI (to stain nuclei) in PBS at room temperature. For IF imaging, tissues were mounted in a custom-made glass-bottom petridish and imaged with a Zeiss LSM 710 laser scanning confocal microscope using a 40x or 63x objective.

IF imaging of *Euprymna scolopes* Animals were cultured and samples were prepared and imaged using IF staining, laser scanning confocal microscopy, and transmission electron microscopy (TEM) as described previously [3].

S.1.2 Image Analysis

Measurement of duct lumen diameter and cilia-to-lumen ratio. Duct lumen (DL) diameter H and cilia-to-lumen ratio h/H were determined from own imaging data (Fig. 1, Extended Data Fig. 1 and 4) and micrographs found in literature (Supplementary Table 1). Two different methods were used for quantitative image analysis, depending on cilia orientation (Extended Data Fig. 3A). In perpendicularly ciliated ducts, which are typically carpets (Extended Data Fig. 3B, left) and only rarely present as highly occluded ducts (Extended Data Fig. 3B, right), h/H was determined as the ciliary layer height h divided by DL diameter H. To quantify H, we identified images that showed the duct in its full width or cross-section and directly measured the diameter. To quantify h, we identified images that showed close-ups of the ciliated carpet in cross-sectional or 3D perspective and we measured cilia length. Given H and h, the cilia-

to-lumen ratio h/H is determined straightforwardly. Since perpendicularly ciliated ducts are assumed to line both "floor" and "ceiling" of the ciliated lumen, h corresponds to twice the cilia length.

In longitudinally ciliated ducts, which are typically flames (Extended Data Fig. 3C, right) and only rarely feature sparsely ciliated designs (Extended Data Fig. 3C, left), the cilia are aligned longitudinally to the DL, and hence cilia density across the channel determines the cilia-to-lumen ratio, rather than cilia length. Thus, h/H was determined from the summed cross-sectional area of all cilia divided by the total cross-sectional area of the DL. For this, cross-sectional images of the duct were identified and thresholded to generate a binary image with cilia cross-sections indicated by white pixels and "empty" lumen by black pixels. Then, h/H was computed by dividing the cilia cross-sectional area (white pixels) by the total cross-sectional area of the DL (black and white pixels) and taking the square root.

Animal phyla excluded from the analysis. As indicated in Supplementary Table 1, phyla were excluded if literature suggested (1) absence of ducts with motile cilia (*e.g.*, Arthropoda, Orthonectida, Placozoa, Tardigrada, Xenacoelomorpha), (2) absence of any motile cilia (*e.g.*, Nematoda, Nematomorpha), or (3) ciliated duct geometries that could not be accurately described with parameters h and H (*e.g.*, Porifera).

Classification using machine learning. We conducted machine learning using the Decision Tree function with cross-validation in the Classification Learning App in Matlab (Mathworks, MA, USA). Five morphometric parameters (duct diameter and length, cilia length and orientation, and cilia-to-lumen ratio) were used to predict bulk transport versus filtration/valve function, where known (Supplementary Table 1). Results are shown in Fig. 2A and S1A.

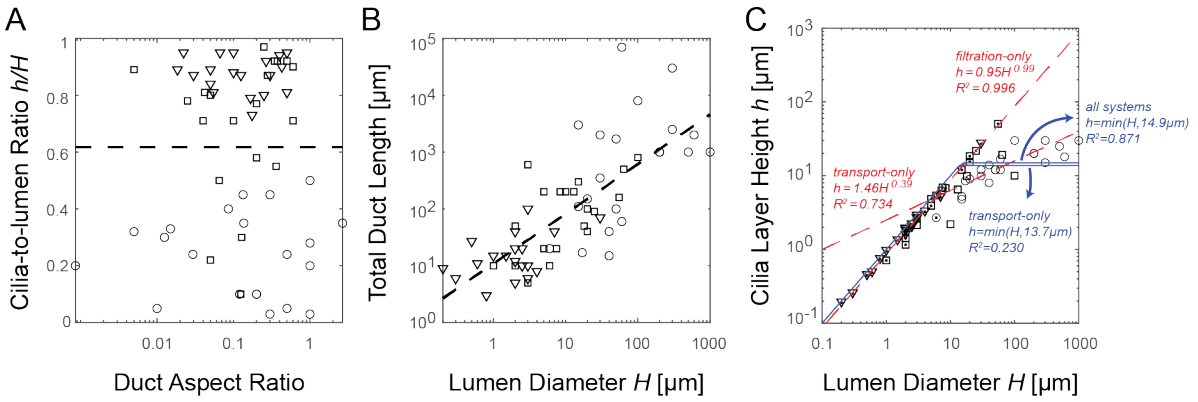

Figure S1: **Relationship of other morphometric parameters.** **A**, cilia-to-lumen ratio h/H versus the duct aspect ratio – lumen diameter H over total duct length with machine learning classification line overlayed. **B**, total duct length versus lumen diameter H in log-log scale with a power law fit overlayed. **C**, different least-squares fits of cilia layer height h as a function of lumen diameter H. The symbols follow that of Fig. 2: ○ for ciliated ducts with confirmed transport/mixing function, ▽ for filtration, and □ for unknown function.

Total duct length and duct aspect ratio. We visualize the relationship between cilia-to-lumen ratio h/H and lumen diameter H to the other recorded morphometric parameter total duct length. In Fig. S1)A, we see that adding duct length information in the form of a dimensionless duct aspect ratio (total duct length over lumen diameter) does not reveal any additional relationship other than what is revealed by the classification using h/H alone discussed above. We believe this is because there is a simple, albeit noisy, correlation between duct length and lumen diameter, as shown by the power law fit line in Fig. S1B ($\log(L) = 0.87\log(H) + 1.04, R^2 = 0.568$).

Least-square fitting of cilia layer height as a function of lumen diameter. We show in Fig. S1C different least squares fits for cilia layer height h as a function of lumen diameter H using all surveyed systems If there exists a universal limit on how long cilia can grow, h should follow the functional form of $\min(h_{max}, H)$, since presumably cilia longer than lumen diameter will bend or buckle. Using all surveyed data together, this model give s fit with $h_{max} = 14.9$ [μm] with $R^2 = 0.8709$. However, this high coefficient of determination is misleading: If we

only look at ducts with known bulk transport function, such a model can only produce a fit with $R^2 = 0.2303$ with $h_{max} = 13.7$ [μm]! However, using simple power-law fit commonly used for scaling-law analysis in biology, we can reach a fit of $R^2 = 0.7342$ with $h = 1.458H^{0.393}$ for bulk transport ducts and $R^2 = 0.9956$ with $h = 0.946H^{0.985}$ for ducts with known filtration functions (compared to $R^2 = 0.9804$ using $h = \min(27.0[\mu m], H)$). Therefore, we conclude that there exists a non-trivial relation that prompt cilia to growth to particular fraction of their ciliated ducts, and use our mathematical model to explore if there is a selection for pumping efficiency based on flow physics in addition to phylogenetic constraints. Trend lines discussed here are labeled in Fig. S1C.

S.2 Physics-based Modeling of Ciliary Ducts

We start by solving the Stokes' equation for u_z^l in the central free lumen

$$\frac{\mu}{r}\frac{\partial}{\partial r}\left[r\frac{\partial u_z^l(r)}{\partial r}\right] = \frac{\partial p}{\partial z}, \qquad \text{for } 0 \leq r \leq a. \tag{1}$$

with finite velocity $u_z^l(0)$ at the center $r = 0$ and matching velocity at $r = a$,

$$u_z^l(a) = \varphi u_z^c(a), \tag{2}$$

where φ is the isotropic fluid fraction inside the porous layer. Here, we assumed that the downstream velocity of the solids (cilia motion averaged over beat cycles) inside the porous ciliary layer is zero at leading order, similar to the infinitesimal analysis of channel flow with passive porosity in [4]. This assumption is also consistent with the notion that f_c is the pressure gradient generated by the cycle-averaged ciliary forces pointing downstream in a confined pipe [5]. The analytical solution to Eq. (1) subject to the boundary condition in (2) is given by

$$u_z^l(r) = -\frac{\partial p}{\partial z}\frac{1}{4\mu}(a^2 - r^2) + \varphi u_z^c(a), \qquad \text{for } 0 \leq r \leq a. \tag{3}$$

The shear stress at the interface $r = a$ when approached from the free lumen side is given by

$$\sigma_{z,f}(a) = \mu \frac{\partial u_z^l}{\partial r}\bigg|_{r=a} = \frac{a}{2}\frac{\partial p}{\partial z}. \tag{4}$$

By continuity $\sigma_{z,p}(a) = \varphi\sigma_{z,f}(a)$ of shear stress $\sigma_{z,p}$ and $\sigma_{z,f}$ at $r = a$ [4, 6], we get

$$\mu \frac{\partial u_z^c}{\partial r}\bigg|_{r=a} = \varphi\frac{a}{2}\frac{\partial p}{\partial z}. \tag{5}$$

The Brinkman equation in the ciliary layer is given by

$$\frac{\mu}{r}\frac{\partial}{\partial r}\left[r\frac{\partial u_z^c(r)}{\partial r}\right] = \varphi\frac{\partial p}{\partial z} + K_c u_z^c(r) + f_c, \qquad \text{for } a \le r \le R, \tag{6}$$

subject to (5) and the no-slip boundary condition at the duct wall $u_z^c(R) = 0$. The analytical solution of (6) is given by

$$\begin{aligned} u_z^c(r) = &\left[2\left(\mathrm{I}_1(\hat{a})\mathrm{K}_0(\hat{R}) + \mathrm{K}_1(\hat{a})\mathrm{I}_0(\hat{R})\right)\right]^{-1} \\ &\left[2(\tilde{f} - \delta p)\left[\mathrm{I}_1(\hat{a})\left(\mathrm{K}_0(\hat{R}) - \mathrm{K}_0(\hat{r})\right) + \mathrm{K}_1(\hat{a})\left(\mathrm{I}_0(\hat{R}) - \mathrm{I}_0(\hat{r})\right)\right]\right. \\ &\left. - \hat{a}\delta p\left[\mathrm{I}_0(\hat{R})\mathrm{K}_0(\hat{r}) - \mathrm{I}_0(\hat{r})\mathrm{K}_0(\hat{R})\right]\right], \qquad \text{for } a \le r \le R, \end{aligned} \tag{7}$$

where $\hat{(\cdot)} = \sqrt{\frac{K_c}{\mu}}(\cdot)$, $\delta p = \frac{\varphi}{K_c}\frac{\partial p}{\partial z}$, $\tilde{f} = \frac{f_c}{K_c}$, and $\mathrm{I}_{(\cdot)}, \mathrm{K}_{(\cdot)}$ are modified Bessel functions of order $(\cdot)$.

Note that since Equation (7) is linear in δp and $\tilde{f}$, we only need to compute solution $U_c = u_z(\tilde{f} = 1, \delta p = 0)$ and $U_p = u_z(\tilde{f} = 0, \delta p = 1)$ and obtain $u_z(\tilde{f}, \delta p) = \tilde{f}U_c + \delta p U_p$.

It is interesting to note that for $\partial p/\partial z = 0$, u_z becomes independent of a as $R \to \infty$. In other words, at zero adverse pressure, the cilia driven flow speed becomes independent of h/H for large H. This trend dictates the existence of an optimal efficiency at small adverse pressure because the amount of active material increases with higher h/H.

S.3 Effective parameter selection

Setting lower limit of the cilia solid fraction φ_c in the ciliary carpet layer. We seek an estimate of the cilia solid fraction φ_c within the ciliary carpet layer. Since the cilium diameter and inter-cilium spacing are roughly equal (about 0.2 μm), in a uniformly-covered ciliated tissue, the expected cilia density should be about $\varphi_c = 0.5^2 \equiv 25\%$. However, many ciliary carpets contain both ciliated and non-ciliated cells, such that the tissue-level coverage fraction of ciliated cells is much less than 100%. In mouse trachea, the ciliated cell coverage can be as low as 37% [7], and amphibian ciliated skin exhibits a 50% ciliated cell coverage [8]. Additionally, individual ciliated cells can have partial ciliation, such as in ependymal epithelia in mammalian brain ventricles where the ciliated area overall approaches only 32% of total surface [9, Fig. 3]. Thus, the overall cilia density, accounting for this heterogeneity in surface coverage is far less than 25%. For example, a tissue with 30%–50% coverage fraction, at 25% cilia density within the covered patches would have an overall cilia density of about 7.5%–12.5%. Thus, we used $\varphi_{c,min} = 10\%$ as a lower bound for our cilia solid fraction (see Fig. 3E of the main text). Together with the ansatz $\varphi_c = h/H$ for observed ciliary flame systems, we use a softplus function $0.1\log(1 + \exp(10(h/H - \varphi_{c,min}))) + \varphi_{c,min}$ to represent φ_c for all values of h/H regardless of the ciliated duct type.

Setting dimensional scale of the active force density f. To calibrate the correct order of magnitude for f, we used measurements of pumping performance in the ciliary flames that connect the peritoneal cavity to the vasculature and filter lymphatic in the toad *Bufo marinus* and *Bufo bufo* [10, 11]. This filtration system consists of 600–800 ciliated flames. Flames exhibit circular and elliptical apertures between 7–40 μm in diameter [10]. Although openings as large as 100 μm were reported, many larger flames appeared to have flap covers that would reduce their “hydrodynamic" diameter [10, Fig.4]. No clear length was visible or reported in

[10], but similar ciliary flames have lengths of at least 30 μm [11, Fig. 7c]. By measuring the pressure difference between the peritoneal and the blood compartment, the authors of [10] reported a maximum flow rate of 0.5$\pm$0.03 ml/hr, a flow rate of 0.17 ml/hr at about 200 Pa, and a maximum pressure of 310 ± 20 Pa (see [10, Fig. 12]). A summary of these measurements is given in Table S2. As a side note, in our survey of ciliated organs in Fig. 2 of the main text, we used a specific *Bufo marinus* funnel of $H = 7$ μm and $h/H = 0.73$ shown in [10, Fig.11] due to its clear visualization of cilia density. To calibrate our model and estimate the force density, we considered in the context of our model the specific example of a ciliated flame of average lumen diameter 15 μm and length 100 μm. We used the measured cilia-to-lumen ratio of $h/H = 0.73$ and the parameter values $\kappa/\mu = 1$ μm^{-2} and $\mu = 10^{-3}$ Pa·s corresponding to the viscosity of water. Our model predicted that this funnel matches the maximum pressure of about 300 Pa observed in [10] if we set the active force density to $f = 15$ pN/μm^3. This value is well within the mechanical capability of cilia averaged over a stroke cycle, given that the internal motors of a single respiratory cilium can generate about 60 pN of force during its effective stroke at the tip, implying a force density of nearly 200 pN/μm^3 for a 200 nm wide, 10 μm long cilium [12]. To further verify the validity of the estimate of $f = 15$ pN/μm^3 for flames of dimensions 100 μm $\times$ 15 μm and $h/H = 0.73$, we calculated that a total of 800 such flames produce a flow rate of about 0.16 ml/hr against 200 Pa of pressure with a maximum attainable flow rate of about 0.46 ml/hr, which are very close to the experimentally reported flow rates. A comparison of experimental data and our model predictions are available in Table. S2. As noted in § S.2, because the final flow field solution depends linearly on the ratio f_c/K_c, any choice of force density scale f indepdendent of h/H and H will not alter the optimality trends computed by our method. Therefore, it is also sensible to consider flow speed/rate derived using our model with other values of f, where the effective forward pressure gradient generated by cilia activity is known to be different, possibly due to changes in unmodeled, microscopic details of the cilia

Filter Type (organism)	Sustainable Pressure [kPa]	Total Filtration Rate [mL/hr]	Unit Size (L x Ø) [μm]	Unit Volume [μL]	Number of Units Required	Total Volume [μL]
Blood-pressure-based Filter (Human kidney glomeruli)	5 – 10	7500	N/A	0.006	1,000,000	6,000
Cilia-powered Filter (*B. marinus* peritoneal flame)	0.29 – 0.33	0.17 @ 200 Pa	unknown x 7 – 40	unknown	600 – 800	unknown
Cilia-powered Filter (simulated)	0.3	0.16 @ 200 Pa	100 x 15	0.00002	800	0.01
Larvacean Ciliated Funnel (*Bathochordaeus sp.*)	0.2	0.4 @ 100 Pa	160 x 55	0.0004	N/A	N/A
Cilia-powered "human kidney"	10	7500 @ 5 kPa	8000 x 55	0.02	20,000,000	400,000

Table S2: **Pumping characteristics of observed and simulated filtration systems.** We list the structural and functional parameters found in literature (black) and derived based on our model (blue). Data for human kidney glomeruli are approximated from [13, 14]. Data from the cilia powered peritoneal filtration in *Bufo marinus* are based on [10]. In all simulations, we used $f = 15$ pN/μm^3, $\kappa/\mu = 1$ μm^{-2}, and $\mu = 10^{-3}$ Pa·s.

coordination or beat waveforms.

Effect of changing the effective Brinkman coefficient $K_c = \kappa\varphi_c$. Since the Brinkman drag coefficient is fundamentally empirical for geometrically complex systems [15, 16], we assumed for simplicity that κ is of the same order as the fluid viscosity throughout the main text of our study. However, since $\sqrt{\mu/\kappa}$ can also be interpreted as an effective pore size for the porous layer [17], it is interesting to see how changing κ would affect the results of our optimization algorithm (Supplementary Algorithm S1). In Fig. S2, we show that increasing the relative value of κ/μ (decreasing the effective pore size) decreases the lumen diameters that maximize the pumping efficiency E. Importantly, all values of κ produce the same relationship between the value of adverse pressure gradient $\mathrm{d}p/\mathrm{d}z$ and cilia-to-lumen ratio h/H, implying that different values of κ would only move the most efficient designs (solid white lines in Fig. 4B or solid black lines in Fig. 4C-D) laterally in the $(H, h/H)$ morphospace;see Fig. S2B. This effect adds another reason why some of the biological ciliated ducts deviates laterally from the most ef-

Algorithm S1 Evaluating performance of duct designs on the morphospace $(H, h/H)$ and identifying optimal duct designs that maximize efficiency E under adverse pressure.

Require: list of ciliated duct morphological parameters:
$(H, h/H)$ // morphospace formed by lumen diameters and cilia-to-lumen ratios
$\mu, f, \varphi_c(H, h/H)$ // fix viscosity, active force scale and forms for cilia solid fraction.

for $\kappa/\mu = 0.1, 1, 10$ **do**
  Pre-compute the following and store each as a matrix over the morphospace $(H, h/H)$:
    $U_c \equiv U_z(H, h/H)$ for $f = 1, \mathrm{d}p/\mathrm{d}z = 0$ // flow velocity due to unit cilia activity
    $U_p \equiv U_z(H, h/H)$ for $f = 0, \mathrm{d}p/\mathrm{d}z = 1$ // flow driven by unit adverse pressure
    $A_c \equiv \frac{1}{4}\pi\varphi_c H^2(1 - (1 - h/H)^2)$ // total ciliated area per cross section
  Compute maximum possible pressure and flow rate generation over $(H, h/H)$:
  $Q^* \equiv \frac{1}{4}\pi H^2 U_c$ // Maximum flow rate occurs when adverse pressure is absent.
  $\mathrm{d}p/\mathrm{d}z^* \equiv -f \cdot U_c/U_p$ // Maximum pressure is generated when net flow is zero.
  Initialize null relative efficiency score over the entire morphospace $(H, h/H)$:
    $E_{\text{rel}} \equiv \textbf{zeros}(H, h/H)$
  for $\mathrm{d}p/\mathrm{d}z = 10^{-10}, \ldots, 10^2$[Pa/$\mu$m] **do**
    $U = f \cdot U_c + \mathrm{d}p/\mathrm{d}z \cdot U_p$ // Compute average flow speed at given adverse pressure.
    if max$(U) < 0$ **then**
      break // Quit if no design parameters can pump at this $\mathrm{d}p/\mathrm{d}z$.
    $E = Q/A_c = \frac{1}{4}\pi H^2 U/A_c$ // Compute efficiency at given adverse pressure.
    Identify optimal designs at given $\mathrm{d}p/\mathrm{d}z$:
      $[E^\dagger, (H, h/H)^\dagger] = \textbf{max}(E)$ // Find design parameters that maximize efficiency
      $E_{\text{rel}} = \textbf{max}(E_{\text{rel}}, E/E^\dagger)$ // Accumulate relative efficiency score
      return $(H, h/H)^\dagger$ // Return optimal design parameters as function of $\mathrm{d}p/\mathrm{d}z$.
  return $Q^*, \mathrm{d}p/\mathrm{d}z^*, E_{\text{rel}}$ // Return quantities as function of κ/μ.

ficient line obtained for the value $\kappa/\mu = 1[\mu m^{-2}]$ (Fig. S3A); they could be more efficient for a different value of effective pore size. Lastly, because predicted h/H remain invariant for all choices of κ, the log-log slope between the cilia layer height h and lumen diameter H for the most efficient systems is also invariant with respect to κ; we show the computed result for $\kappa/\mu = 1[\mu m^{-2}]$ in Fig. S3B. Note that for most lumen diameter values, the predicted slope is comparable to the power law fits of $0.393 \approx 0.4$ shown in Figure 2 and 4 as red dashed lines.

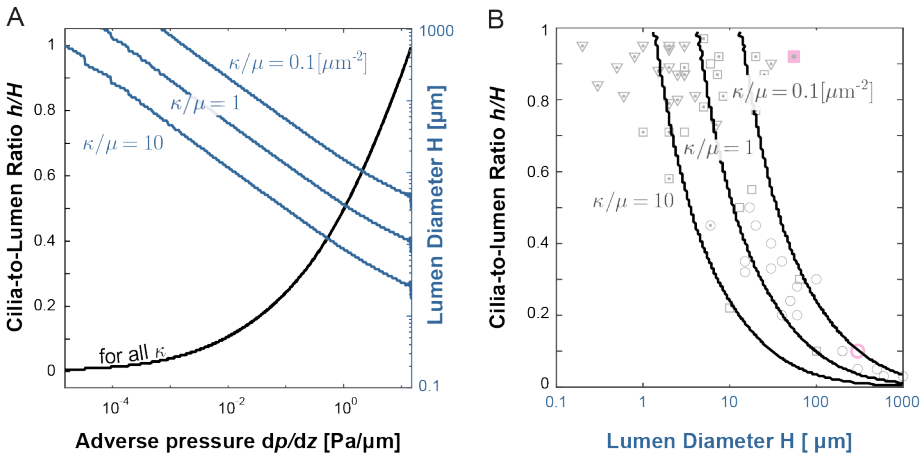

Figure S2: **Effect of Brinkman coefficient κ on morphology of most efficient designs. A.** Result of our optimization (Algorithm S1) for different values of κ while maintaining all other parameters fixed. The most efficient designs have smaller lumen diameter H at a higher hydraulic resistance coefficient κ/μ, but the optimal cilia-to-lumen ratio h/H do not change. **B.** In morphospace, the most efficient designs shift only horizontally for different values of κ. This provides an additional explanation for the lateral spread of the biological data points. Here $\mu = 10^{-3}$ [Pa· s] and $f = 15$ [pN/μ m^3].

S.4 Quantitative comparison of excretory organs

Flame cells serve as a basic filtration unit in many mm-scale organisms, but are markedly absent in larger organisms, (except during some stages of development) [18]. Filtration in larger organisms, the human kidney for example, leverages the blood pressure generated by a muscular heart. We propose that the lack of filtration by ciliary flames in larger animals might be (partly) due to the unfavorable scaling of pressure and flow generation in flame-based filtration compared to blood pressure-based filtration, as the following example illustrates. In humans, the filtration pressure provided by the capillary blood pressure is on the order of $5 - 10$ kPa [13]. The average filtration rate of the kidney is ca. 180 liters of blood per day, which, considering nearly 1,000,000 filtration units (glomeruli) [14], indicates a filtration rate of 7.5 μl/hr per glomerulus. Given an average glomerular volume of $6 \cdot 10^6$ μm^3, the total space taken up by the filtration units is ca. 6 ml [14]. The larvacean's ciliated funnel, the largest ciliary pump

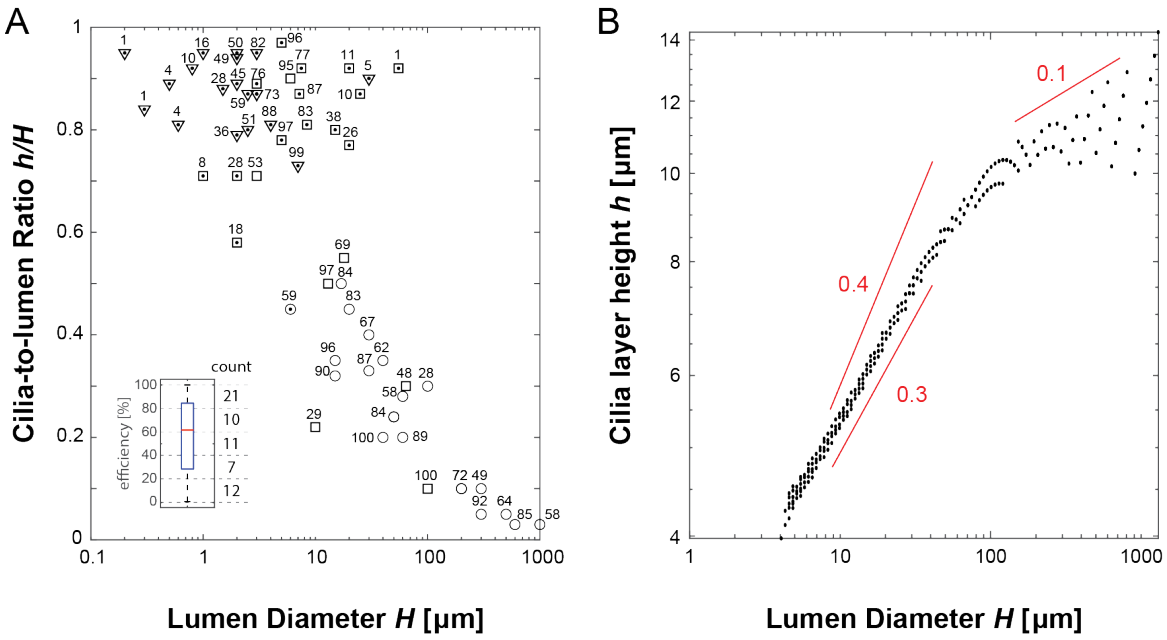

Figure S3: **Predicted efficiency assuming** $\kappa/\mu = 1[\mu m^2]$**. A.** We show the maximum relative efficiency produced by our optimization algorithm at the exact point of morphospace associated with each reported data points. Inset shows the box plot (median indicated in red, box marks the 25th to 75th percentile, and whisker shows the full range) and histogram bin count of the shown efficiency values. **B.** The log-log slope of the computed most efficient systems is between 0.3 and 0.4 for lumen diameter below 100 [μm], and drops to around 0.1 for larger lumen diameters. These slope is invariant with respect to the specific parameter choices. Here $\mu = 10^{-3}$ [Pa· s] and $f = 15$ [pN/μ m^3].

found in our survey, can efficiently pump 0.4 μl/hr of fluid against 0.6 Pa/μm of pressure gradient (Fig. 4A). This means that the parallel operation of ca. 20 such funnels, each with more than 8 mm in length, can produce comparable a flow rate (20×0.4 = 8 μl/hr) at the minimum 5 kPa pressure drop observed across the glomerular filtration barrier. Assuming biologically feasible, such funnel would be able to sustain a maximum pressure at nearly 10 kPa without flow. Using the lumen diameter $H = 55$ μm as a lower bound, the resulting tissue volume that replaces a single glomerulus would measure 0.02 μl, which leads to about 0.4 liters if these funnels were to replace the operation of all 6 ml of glomerular volume in an entire kidney. This example demonstrates the unfavorable scaling of cilia-based filtration to larger body sizes and

their higher filtration rate demands.

References

1. Abràmoff, M. D., Magalhães, P. J. & Ram, S. J. Image processing with ImageJ. *Biophotonics international* **11,** 36–42 (2004).
2. Tinevez, J.-Y. *et al.* TrackMate: An open and extensible platform for single-particle tracking. *Methods* **115,** 80–90 (2017).
3. Essock-Burns, T., Bongrand, C., Goldman, W. E., Ruby, E. G. & McFall-Ngai, M. J. Interactions of Symbiotic Partners Drive the Development of a Complex Biogeography in the Squid-Vibrio Symbiosis. *mBio* **11** (2020).
4. Damiano, E., Duling, B., Ley, K. & Skalak, T. Axisymmetric pressure-driven flow of rigid pellets through a cylindrical tube lined with a deformable porous wall layer. *Journal of Fluid Mechanics* **314,** 163–189 (1996).
5. Liron, N. & Shahar, R. Stokes flow due to a Stokeslet in a pipe. *Journal of Fluid Mechanics* **86,** 727–744 (1978).
6. Hou, J. S., Holmes, M. H., Lai, W. M. & Mow, V. C. Boundary Conditions at the Cartilage-Synovial Fluid Interface for Joint Lubrication and Theoretical Verifications. *Journal of Biomechanical Engineering* **111,** 78–87. ISSN: 0148-0731. `https://doi.org/10.1115/1.3168343` (Feb. 1989).
7. Ramirez-San Juan, G. R. *et al.* Multi-scale spatial heterogeneity enhances particle clearance in airway ciliary arrays. *Nature Physics* **16,** 958–964 (2020).
8. Boselli, F., Jullien, J., Lauga, E. & Goldstein, R. E. Fluid mechanics of mosaic ciliated tissues. *Physical review letters* **127,** 198102 (2021).
9. Mirzadeh, Z., Han, Y.-G., Soriano-Navarro, M., Garcıa-Verdugo, J. M. & Alvarez-Buylla, A. Cilia organize ependymal planar polarity. *The Journal of Neuroscience* **30,** 2600–2610 (2010).
10. Morris, J. L. Structure and function of ciliated peritoneal funnels in the toad kidney (Bufo marinus). *Cell and Tissue Research* **217,** 599–610 (1981).
11. Møbjerg, N., Larsen, E. H. & Jespersen, Å. Morphology of the nephron in the mesonephros of Bufo bufo (Amphibia, Anura, Bufonidae). *Acta Zoologica* **79,** 31–50 (1998).
12. Hill, D. B. *et al.* Force generation and dynamics of individual cilia under external loading. *Biophysical journal* **98,** 57–66 (2010).
13. Rubenstein, D., Yin, W. & Frame, M. D. *Biofluid Mechanics: an Introduction to Fluid Mechanics, Macrocirculation, and Microcirculation* (Academic Press, 2015).

14. Nyengaard, J. & Bendtsen, T. Glomerular number and size in relation to age, kidney weight, and body surface in normal man. *The Anatomical Record* **232,** 194–201 (1992).

15. Nield, D. The Beavers–Joseph boundary condition and related matters: a historical and critical note. *Transport in porous media* **78,** 537–540 (2009).

16. Nield, D. & Kuznetsov, A. An historical and topical note on convection in porous media. *Journal of Heat Transfer* **135,** 061201 (2013).

17. Alvarado, J., Comtet, J., De Langre, E. & Hosoi, A. Nonlinear flow response of soft hair beds. *Nature Physics* **13,** 1014–1019 (2017).

18. Bartolomaeus, T. & Ax, P. Protonephridia and Metanephridia-their relation within the Bilateria. *Journal of Zoological Systematics and Evolutionary Research* **30,** 21–45 (1992).

Supplementary Table 1

INDEX	Phylum	Clade	Common Name	Sub-Group(s)	Species	Cilia Type: Internal motile cilia IC, External motile cilia EC, Flagellated Sperm S	Organ	Orientation to channel axis: Perpendicular (carpet-style) 1; horizontal (flame-style) 2	Function: unknown/else 0, pumping/transport 1, ultrafiltration/pressure/valve 2	Function	References consulted	H [um]	h^2/H^2 (where applicable)	h/H	References consulted	Cilia length [um]	References consulted	Duct length [um]	References consulted	Initial Packing Density [0-1]	Additional comments
1	Annelida	Trochozoa	Ringed or Segmented	Polvchaete worm	Aeolosoma benaalens	IC	Proximal nephridial duct of	2	0	Presumed pumping/valve	Bunke 1994	1	0.5	0.71	Bunke 1994, Fig.4	NA		10	estimate of lower limit (10x of diameter) since Bunke 1994 calls the duct "long"without providing	0.5	
2	Annelida	Trochozoa	Ringed or Segmented Worms	Polychaete worm	Anaitides mucosa	IC	Ciliated funnel parallel to protonephridial duct in adults	2	0	Potential uptake of gametes from coelum	Bartolomaeus 1998	20	0.84	0.92	Bartolomaeus 1998, Fig.6B	15	Bartolomaeus 1998, Table 2	40	Bartolomaeus 1998, Fig. 7B and Fig. 1E (schematic)	0.84	
3	Annelida	Trochozoa	Ringed or Segmented	Polychaete worm		IC	Duct of protonephridia in adults	2	2	Excretion/ Ultrafiltration	Bartolomaeus 1998	2	0.8	0.89	Bartolomaeus 1998, Fig.4G	20	Bartolomaeus 1998, Fig. 1E (schematic)	40	Bartolomaeus 1998, Fig. 1E (schematic)	0.8	
4	Annelida	Trochozoa	Ringed or Segmented Worms	Polychaete worm	Nerillidium rroglochaeroides	IC	Foregut	1	1	Transport of food particles and mucus	Purschke & Tzetlin 1992	20	0.2	0.45	Purschke & Tzetlin 1992, Fig. 4A	10	Purschke & Tzetlin 1992, Fig. 4A & text	150	Purschke & Tzetlin 1992, text	0.5	
5	Annelida	Trochozoa	Ringed or Segmented	Spoon Worm	Thalassema thalassemum	IC	Terminal cell of larvae ("head kidney")	2	2	Excretion/ Ultrafiltration/absorption	Kato 2011	1.5	0.78	0.88	Kato 2011, Fig. 3C text	15	Kato 2011, Fig. 3C, text	15	Kato 2011, Fig. 3C, text	0.78	
6	Brachiopoda	Trochozoa	Lampshells		Lingula anatina	IC	Ciliated internal epithelium of the mantle	1	1	Transport of particles and mucus	Westbroek 1968,Westbroe 1980 (Fig 3, aka plate I)	500		0.05	Westbroek 1980, Plate IA; Forchiell 2012	13	Westbroek 1980 Txt, Plate I Fig C/F	1000	estimated from Gerdol 2018	0.5	
7	Bryozoa	Spiralia			Phylactolaemata	IC	Ciliated trunk coelem	1	0	Presumably nutrient transport (since lack of blood vessels)	Gruhl 2009	10	0.05	0.22	Gruhl 2009, Fig. 4F	3	Gruhl 2009, Fig. 3B	200	estimated entire length of animal, see Gruhl 2009, Fig.1A	0.5	
8	Bryozoa	Spiralia			Phylactolaemata	IC	Forked canal with a sort of flame cell	2	0	Has been suggest to serve for filtering since no excretory organs are known in Bryozoa	Gruhl 2009	5	0.95	0.97	Gruhl 2009, Fig. 2B, 4C,D	10	Gruhl 2009, Fig. 4C,D	20	estimated forked channel length; Gruhl 2009 2A	0.95	
9	Cephalochordata	Chordata		Lancelets	Branchiostoma virginiae, Branchiostoma lanceolatum	IC	Hatschek' s nephridium -filtration cells (cyrtopodocytes)	2	0	Aiding ultrafiltration of the filtering has been proposed (there is ultrafiltration via diaphragms and blood pressure as well) but the cellular structure suggests otherwise - maybe pumping plus absorption (flagellum is surrounded by microvilli)	Ruppert 1996	2	0.34	0.58	Ruppert 1996, Fig.7	10	Brandenburg 1961, Fig. 25	10	Brandenburg 1961, Fig. 25	0.34	
10	Cephalochordata	Chordata		Lancelets	Branchiostoma virginiae	IC	Intestine and colon	1	1	Transport of food particles and mucus		200		0.10	Biuw 1974, Fig.3A (based on cilia length = 10um Kucera 2009, Fig1A	10	Biuw 1974, Fig.3A ; Kucera 2009, Fig1A	1000	estimated from He 2018	0.5	
11	Chaetognatha	Chaetognatha	Arrow worms		Spadella cephaloptera	IC	Intestine	1	1	Transport of particles and mucus	Perez 2000	15	0.1	0.32	Perez 2000, Fig.5 and Perez 2001 Fig 2F	NA		3000	estimated from Perez 2001, Fig. 2B	0.5	
12	Cnidaria	Cnidaria		Octocorals	acrossota amboinensis	IC	Gastrovascular cavity / stolon: Polyps are long and tubular and are interconnected by horizontal tabulae o stolons which form transverse platforms	1	1	Transport/mixing, possibly of cells	Harmata 2013, Fig.6	600		0.03	Harmata 2013, Fig.7	10	Harmata 2013, Fig.4E	2000	at least; estimated from Harmata 2013, Fig. 3	0.5	
13	Craniata	Chordata		Amphibian-Caecilian	Geotrypetes seraphini	IC	Neck segment of mesonephros	2	0	Presumed: excretion/ultrafiltration	Møbjerg 2004, Fig. 5, 8	15.00	0.64	0.80	Møbjerg 2004, Fig. 8A	20.00	estimated from Møbjerg 2004, Fig. 5	300	Møbjerg 2004, text	0.64	
14	Craniata	Chordata		Mammals (human)	Homo sapiens sapiens	IC	Small airways (Specifically, the epithelia pleats)	1	1	Transports mucus up the respiratory tree (Mucociliar clearance)	Bustamante-Marin 2017	50.00		0.24	Flores-Delgado 2015, Fig.1 and 2	6.00	Flores-Delgado 2015, Fig.1 and 2	1700	Weibel 1963	0.5	
15	Craniata	Chordata		Mammals (human)	Homo sapiens sapiens	IC	Fallopian Tube	1	1	Transport of oocytes	Raidt 2015	60.00		0.20	Raidt 2015, Fig. 4 (cilia length); Patek 1974; Varga 2018, Fig. 2 Du dimensions)	6.00	Raidt 2015, Fig. 4	70000	7-11cm; Han 2020	0.5	
16	Craniata	Chordata		Mammals (human)	Homo sapiens sapiens	IC	Tubule of bronchial submucosal gland	1	1	Transport mucus	Meyrick 1969	30		0.40	Meyrick 1969, text and table (cilia length / diameter)	6	Meyrick 1969	350	Meyrick 1969, text and table	0.5	
17	Craniata	Chordata		Mammals (human)	Homo sapiens sapiens	IC	Brain ventricle cilia (ependymal cilia)	1	1	Transport / mixing		1000		0.03	Zhuravlova 2018; Worthington 1963	13	Jiménez 2014; Dempsey 1976	1000	Zhuravlova 2018	0.5	
18	Craniata	Chordata		Mammals (mouse)	Mus musculus	IC	Brain ventricle cilia (ependymal cilia)	1	1	Transport of cerebrospinal fluid and possibly signals/cells	Faubel 2016	#####		0.10	Xiong 2014, Fig. 1A	10.00	Xiong 2014, Fig.2B	1000	Xiong 2014, Fig.1A	0.5	
19	Craniata	Chordata		Mammals (mouse)	Mus musculus	IC	Efferent ductules (male reproductive system)	1	1	Transport of sperm cells; stirring	Lee 2000; Hess 2015	#####		0.30	average from Lambot 2009 and Yua 2019, Movie S3, Fig.1	17.00	Yuan 2019, Fig.4A and text	8000	Lambot 2009	0.5	
20	Craniata	Chordata		Amphibians (Toad)	Rhinella marina (Bufo marina)	IC	Kidney, peritoneal funnels (connects coelum to nephros)	2	2	Blood volume/osmoregulator regulator: Filters particles and pumps protein-rich peritoneal fluid back into the kidney blood vasculature;	Morris 1981	7.00	0.73	0.85	Morris 1981, Fig. 11	10.00	estimated from Morris 1981, Fig. 10	40	estimated from Møbjerg 2000, Fig.5	0.73	Pressure generated in peritonal funnels: 300 Pascal (Morris 1981)
21	Craniata	Chordata		Amphibians (Toad)	Bufo bufo / viridis	IC	Kidney, neck segment of the mesonephros	2	0	Presumed: excretion/ultrafiltration	Møbjerg 1997, 2001	25.00	0.76	0.87	Møbjerg 1997, Fig.7C	10.00	Møbjerg 1997, Fig. 7C	90	Møbjerg 1998,text	0.76	
22	Craniata	Chordata		Avians - Bird (Ostrich)	Struthio camelus	IC	Uterus folds	1	1	Presumably transport of mucus	Sharaf 2013	30.00		0.33	Sharaf 2013, Fig. 4D	5.00	Sharaf 2013, Fig. 4C	2000	at least; Sharaf 2013, Fig. 4C	0.5	
23	Craniata	Chordata		Reptile (Lizard)	Podarcis sp.	IC	Urinary bladder Stalk	1	0	Unknown - possibly transport of highly viscous or precipitated urine, out of bladder stalk (Bolton &	Bolton & Beuchat 1991	64.00		0.30	Rheubert 2014, Fig. 6.3 (duct diameter(; Bolton & Beuchat 1991, Fig. 1 (cilia)	10.00	estimated from Bolton & Beuchat 1991, Fig. 1	500	Rheubert 2014, Fig.6.3	0.5	
24	Craniata	Chordata		Osteichthyes (Bony Fish)	Danio rerio (72hpf)	IC	Pronephros proximal tubule of metanephridia	2	0	Unknown- Presumed: ultrafiltration	Zhang 2012, Ott 2016, Delaval 2011	3	0.8	0.89	Ott 2016 Fig. 3A+D; Lee 2015, Fig 4G	9	Kramer-Zucker 2005 Fig 1F and Table	600	Vasilyev 2012, Fig.1G and text	0.8	
25	Craniata	Chordata		Osteichthyes (Bony Fish)		IC	Olfactory pit cilia	1	1	Generating flow to nose for chemical sensing	Reiten 2017	60		0.28	Reiten 2017, Fig.1A	9	Reiten 2017, text	60	circular; Reiten 2017, Fig.1A	0.5	
26	Ctenophora	Ctenophora	Comb jellies		Beroe abyssicola	IC	Endodermal (gastrovascular) canal	1	1	Absorption and transport of food	Presnell 2016,Norekian 2019, Tamm 2014, Gemm 1918	300		0.05	Presnell 2016 Movie S4	8	Cilia length ~6-10um, Presnell 2016, Movie S4	30000	estimate from Presnell2016 Fig.1	0.5	
27	Cycliophora	Spiralia			Symbion pandora	IC	Intestine	2	0	Probably absorption and transport	Neves 2009	2	0.5	0.71	Neves 2009, Fig. 5, 4D	NA		50	extremely crude estimate form Neves 2009 Fig.4A	0.5	
28	Dicyemida	Spiralia	Rhombozoa		Dicyema acuticephalum	IC	Urn Cavity in Larvae	1	0	Unknown. Hypothesis: Pump fluid to exchange with outside? Furuya 1997	Furuya 1997,1999, Bresciani 1967, Matsubara 1976	3	0.5	0.71	Furuya 1997, Fig. 10	2	estimated from Matsubara 1976 Fig 8E, text; Bresciani 1967 Fig 1 & Fig. 4	5	estimated from drawings in Furuya 1999	0.5	
29	Echinodermata	Ambulacraria	Echinoderms	Sea Urchin/Sea Star (Echinoids)	Hemicentrotus pulcherrimus, Strongylocentrotus pallidus	IC	Pore canals	1	0	Hypothesis: In relaxed state, pumping of fluid inwards, transport of particles outwards (bi directiona transport)	Tamori 1996, Fergusson 1990, 1991, 1996	13.00	0.25	0.50	Tamori 1996; Fig. 7a and text	12	Tamori 1996, Fig.8	200	Tamori 1996, Fig.5	0.5	
30	Echinodermata	Ambulacraria	Echinoderms	Sea Urchin	Hemicentrotus pulcherrimus	IC	Pore canals	2	0	Hypothesis: in contracted state, maintain hydrostatic pressure (for tube feet), ultrafiltration	Tamori 1996	8.40	0.65	0.81	Tamori 1996	12	Tamori 1996, Fig. 8	200	Tamori 1996, Fig.5	0.65	
31	Entoporcta	Spiralia	Goblet worms		Loxosomatoides	IC	Esophagus	1	1	Presumably transport/mixing	Schwaha 2010	15		0.35	Schwaha 2010, Fig.4c	3.3	Schwaha 2010, Fig. 4c	110	Schwaha 2010, Fig. 4c	0.5	
32	Entoporcta	Spiralia	Goblet worms		sirindhornae; Umatella gracilis	IC	Terminal cells of protonephrida	2	2	Excretion/ Ultrafiltration	Schwaha 2010; Kuemmel 1962	2.5	0.75	0.87	Schwaha 2010, Fig. 3e and f (H); Kuemmel,Fig.10,(h/H)	20	Schwaha 2010, Fig. 3e and f	20	length of filtration zone (estimated from diameter/length ratio in Kuemmel Fig 8)	0.75	
33	Gastrotricha	Spiralia	Hairyback		Chaetonotus maximus	IC	Terminal cells of protonephrida	2	2	Excretion/ Ultrafiltration	Kieneke 2008; Fontaneto 2015	0.5	0.8	0.89	Kieneke 2008, Fig 10c; Fontaneto 2015 Fig 1.30 B	27	Kieneke 2008, text and Fig 9b	27	Kieneke 2008, text and Fig 9b	0.8	No evidence of carpet style ducts except potentially in pharynx of Dendroadasys affinisgracilis but no imaging data is available (Kieneke 2015)
34	Gnathostomulida	Gnathifera	Jaw worms		Gnathostomula paradoxa	IC	Terminal cells of protonephrida	2	2	Blood volume/osmoregulator regulator: Filters particles and pumps protein-rich peritoneal fluid back into the kidney blood vasculature;	Lammert 1985	0.6	0.65	0.81	Lammert 1985, Fig. 2C	11	Lammert 1985, text	11	Lammert 1985, text	0.65	No evidence of perpendicularly ciliated ducts in this phylum
35	Hemichordata	Ambulacraria	Acorn worm		Meioglossus psammophilus	IC	Mid gut	1	1	Transport of food	Worsaae 2012	50		0.24	Worsaae 2012, Fig. 5A; Movie S2	6	Worsaae 2012, Fig. 5A; Movie S2	100	Worsaae 2012, Fig. 5A	0.5	No evidence of longitudinally ciliated ducts in this phylum except potentially the ciliated canal-hydropore in the larvae but imaging data of cilia are not available (Ruppert 1996)
36	Kinorhyncha	Scalidophora	Mud dragons		Pycnophyes kielensis	IC	Terminal cells of protonephrida	2	2	Excretion/ Ultrafiltration	Neuhaus 1988	2	0.9	0.95	Neuhaus 1988, Fig.4C, 5C	20	Neuhaus 1988, estimated from Fig.1A	20	Neuhaus 1988, estimated from Fig.1A	0.9	No evidence of perpendicularly ciliated ducts in this phylum
37	Loricifera	Scalidophora	Brush heads		Armorloricus elegans	IC	Terminal cells of protonephrida	2	2	Excretion/ Ultrafiltration	Neuhaus 2007	0.2		0.95	(1 cilium) Neuhaus 2007, Fig. 4B	9	Neuhaus 2007, Fig 3A and text	9	Neuhaus 2007, Fig 3A and text	0	No evidence of perpendicularly ciliated ducts in this phylum
38	Micrognathozoa	Gnathifera			Limnognathia maerski	IC	Terminal cells of protonephrida	2	2	Excretion/ Ultrafiltration	Kristensen 2000	0.3	0.7	0.84	Kristensen 2000, Fig.30 & 31 (average of 4 Terminal cells)	6	Kristensen 2000, Fig.30	6	Kristensen 2000, Fig.30	0.7	No evidence of perpendicularly ciliated ducts in this phylum
39	Mollusca	Trochozoa	Mollusks	Blue Mussel	Mytilus edulis	IC	Lateral Gill Cilia	1	1	Fluid pumping for filter feeding (particles of 4um or more)	Riisgard 1996, 2015	40		0.35	Riisgard 2015 ,Fig.4c; Riisgard 1996 Fig 2	15	Riisgard 2015, text	15	width of ridge; Riisgard 2015, text	0.5	
40	Mollusca	Trochozoa	Mollusks	Bobtail squid	Euprymna scolopes	IC	Proximal ciliated duct that leads to cysts in light organ	1	0	Potentially interaction with symbionts	Essock-Burns 2020	18		0.55	Essocks-Burns 2020	5	Essocks-Burns 2020	50	Essocks-Burns 2020 Fig. 2A	0.5	
41	Mollusca	Trochozoa	Mollusks	Bobtail squid	Euprymna scolopes	IC	Bottleneck of ciliated duct that leads to cysts in light organ	1	0	Potentially interaction with symbionts	Essock-Burns 2020	6		0.90	Essocks-Burns 2020	3	Essocks-Burns 2020	10	Essock-Burns 2020 Fig. 3A/B	0.5	
42	Mollusca	Trochozoa	Mollusks	Chiton	Lepidochitona corrugata (juvenile)	IC	Ciliary flame of protonephridia	2	2	Excretion/ Ultrafiltration	Baeumler 2011	4	0.65	0.81	Baeumler 2011, Fig 6D	8	Baeumler 2011, Fig 6D	8	Baeumler 2011, Fig 6D	0.65	
43	Mollusca	Trochozoa	Mollusks	Chiton	Lepidochitona corrugata	IC	Renopericardial duct of metanephridia	2	0	Unknown	Baeumler 2012	5	0.61	0.78	Baeumler 2012. Fig.9C	NA		200	Baeumler 2012. Fig.7G	0.61	
44	Nemertea	Trochozoa	Ribbon worms		Lineus viridis, Carinoma mutabilis	IC	Terminal cells of protonephridia	2	2	Excretion/ Ultrafiltration	Bartolomaeus 1985, 2014	1	0.9	0.95	Bartolomaeus 1985, Fig. 3D; Bartolomaeus 2014; Fig 2B	15	Bartolomaeus 2014 text	15	Bartolomaeus 2014 text	0.9	No evidence of carpet style ducts
45	Onychophora	Panarthropoda	Velvet worms		Ooperipatellus decoratus, Euperipatoides rowelli	IC	Oviduct	1	0	Probably oocyte and embryo transport	Brockmann 2001, Curach 1999	100		0.10	estimated from Curach 1999, Fig. 1	NA		800	Brockmann 2001, text	0.5	
46	Onychophora	Panarthropoda	Velvet worms		Peripatopsis sp.	IC	Neohrostome of metanephridium	2	0	Probably absorption and transport	Storch 1978, Mayer 2006	20	0.6	0.77	Storch 1978, Fig.4; Mayer 2006,	NA		100	Mayer 2009, Fig.10B	0.6	
47	Phoronida	Trochozoa	Horseshoe worm		Phoronis muelleri (larvae)	IC	Protonephridial duct	2	2	Excretion/ Ultrafiltration	Bartolomaeus 1989	3	0.75	0.87	Bartolomaeus 1989, Fig.1B and 2	10	Bartolomaeus 1989, Fig.1B and 2; Hay-Schmidt 1987, Fig.18	100	Hay-Schmidt 1987 text	0.75	
48	Phoronida	Trochozoa	Horseshoe worm		Actinotrocha vancouverensis (larvae)	IC	Midgut	1	1	Food transport	Temereva 2010	40		0.20	Temereva 2010, Fig. 2	4	Temereva 2010, Fig. 2	40	Temereva 2010, Fig. 2	0.5	
49	Platyhelminthes	Spiralia	Flatworm	Planarian	Artiopostha sp	IC	Terminal cell/proximal ductule of protonephridia	2	2	Excretion/ Ultrafiltration	Rohde 1992, McKanna 1968	2.00	0.88	0.94	Rohde 1992, Fig. 13 &15; McKanna 1968 , Fig. 2	5	McKanna 1968 , Fig.1 and text	5	McKanna Fig.1	0.88	No evidence of carpet style ducts
50	Platyhelminthes	Spiralia	Flatworm	Planarian	Artiopostha sp	IC	Distal collecting duct of protonephridia	2	1	Transport	Rohde 1992, McKanna 1969	6.00	0.2	0.45	Rohde 1992, Fig.14&16 ; McKanna 1968, Fig.9 and 10	5	McKanna 1968 , Fig.1 and text	20	McKanna Fig.1	0.2	
51	Platyhelminthes	Spiralia	Flatworm	Planarian	Schmidtea mediterranea	IC	Terminal cell of protonephridia	2	2	Excretion/ Ultrafiltration	Vu 2015	3.00	0.75	0.87	Vu 2015, Fig.4D and Fig.1B	10	Rink 2011, Fig. 1D & 2D	10	Rink 2011, Fig. 1D & 2D	0.75	
	Platyhelminthes	Spiralia	Flatworm	Tapeworm	Taenia solium	IC	Terminal cell of protonephridia	2	2	Excretion/ Ultrafiltration	Valverde-Islas 2011	3.00	0.9	0.95	Valverde-Islas 2011 Fig. 2G & 5C	6.00	Valverde-Islas 2011, Fig. 2G	6	Valverde-Islas 2011, Fig. 2G	0.9	
53	Priapulida	Scalidophora	Penis worms		Meiopriapulus fijiensis	IC	Protonephridia with multiple terminal cells	2	2	Ultrafiltration for osmolar balance	Storch 1989	2.5	0.64	0.80	Storch 1989, Fig. 26-17	10	estimated from Storch 1989, Fig. 31	10	estimated from Storch 1989, Fig. 31	0.64	No evidence of perpendicularly ciliated ducts in this phylum
54	Rotifers	Gnathifera	Wheel animals		Habrotrocha rosa	IC	Terminal cell of protonephridia	2	2	Ultrafiltration for osmolar balance	Schramm 1978	0.8	0.85	0.92	Schramm 1978, Fig.2d-f	3	Schramm 1978, Fig.2a and text	3	Schramm 1978, Fig.2a and text	0.85	
55	Rotifers	Gnathifera	Wheel animals		Asplanchna	IC	Terminal cell of protonephridia	2	2	Ultrafiltration for osmolar balance	Warner 1969	2	0.62	0.79	Warner 1969, Fig.6 and 9	12	Warner 1969, text	12	Warner 1969, text	0.62	
	Rotifers	Gnathifera	Wheel animals		Brachionus olicatilis	IC	Stomach	1	1	Transport, Absorption	Yu 1979, Ma 2022	17		0.50	Ma 2022, Fig. 2A	5	Ma 2022, Fig. 2A	17	Ma 2022, Fig. 2A	0.5	
57	Urochordata	Chordata		Larvacean (tunicates)	Bathochordaeus stygius	IC	Esophagus	1	1	Transport of food particles	**Data in this manuscript**	300		0.10	**Data in this manuscript**	15	**Data in this manuscript**	2500	**Data in this manuscript**	0.5	
58	Urochordata	Chordata		Larvacean (tunicates)	Bathochordaeus stygius	IC	Ciliated duct (neurohypophyseal duct)	2	0	Unknown. Hypothesis I: Ultrafiltration: Pumps and filters external seawater into blood sinus to maintain hydrostatic pressure/blood volume (Ruppert 1996). Hypothesis II: structure corresponds to adenohypophysis (Boorman 2002, Holmberg 1982,	**Data in this manuscript** and Ruppert 1996, Deyts 2006, Boorman 2002, Holmberg 1982, Manni 2005	55.00	0.85	0.92	**Data in this manuscript**; Sherlock 2016, Fig.4	100	**Data in this manuscript**	160	**Data in this manuscript**; Sherlock 2016, Fig.4	0.85	

59	**Urochordata**	**Chordata**		Larvacean (tunicates)	Oikopleura dioica	IC	Ciliated duct (also called ciliary funnel, neurohypophyseal duct or olfactory funnel)	2	0	Unknown. Hypothesis I: Ultrafiltration: Pumps and filters external seawater into blood sinus to maintain hydrostatic pressure/blood volume (Ruppert 1996). Hypothesis II: structure corresponds to adenohypophysis (Boorman 2002, Holmberg 1982,	Ruppert 1990, Deyts 2006, Boorman 2002, Holmberg 1982, Manni 2006	7.5	0.85	0.92	Holmberg 1982, Fig.9	20	**Braun 2016, Fig. 5D;** Holmberg 1982, Fig.1	20	Braun 2016, Fig. 5D; Holmberg 1982, Fig.1	0.85	
60	**Urochordata**	**Chordata**		Larvacean (tunicates)	Oikopleura dioica	IC	Esophagus-to-Stomach valve (called "Cardiac Valve" in paper)	2	2	Valve-function: Preventing reflux of food	Lopez-Urrutia & Acuña 1999, Burighel 2001	30	0.81	0.90	Burighel 2001, Fig. 3D	20	Burighel 2001, Fig. 3D	70	Burighel 2001, Fig. 3D	0.81	
61	**Urochordata**	**Chordata**		Ascidian (tunicates)	Ascidia interrupta	IC	Ciliated duct (also called ciliary funnel, neurohypophyseal duct or olfactory funnel)	2	0	Unknown. Hypothesis I: Ultrafiltration: Pumps and filters external seawater into blood sinus to maintain hydrostatic pressure/blood volume (Ruppert 1996). Hypothesis II: structure corresponds to adenohypophysis (Boorman 2002, Holmberg 1982,	Ruppert 1990, Deyts 2006, Boorman 2002, Holmberg 1982, Manni 2007	7.2	0.75	0.87	Ruppert 1990, Fig.8	NA	Ruppert 1990, Fig.8	NA		0.75	
Excluded Phylae																					
62	**Anthropoda**		**Anthropods**	Insects, spiders, crustaceans etc		No motile cilia in larvae and adults, except S; Buchsbaum 1987															
63	**Nematoda**		**Roundworms**			No motile cilia (only sensory); Apfeld & Kenyon 1998															
64	**Nematomorpha**		**Gordian worms**			No motile cilia (only sensory), Hanelt 2005															
65	**Orthonectida**		**Orthonectids**			EC but no internal motile cilia; indeed no anatomically recognized digestive, circulatory, or excretory systems; Zverkov 2019															
66	**Placozoa**			Placozoa	Trichoplax	EC but no internal motile cilia; indeed no anatomically recognized digestive, circulatory, or excretory systems;															
67	**Porifera**		**Sponges**			Other (many parallel high pressure ciliated pumps that together generate high flow) ; Leys 2006/2011; Dunn															
68	**Tardigrada**		**Water bear**			S and sensory (non motile cilia), Bonifacio 2012, Suzuki 2014															
69	**Xenacoelomorpha**				Xenoturbella sp.	EC,S, but no IC. Largely lacking discrete organs (e.g., without a discrete circulatory system, nephridia, or organized gonads); Brusca, 2016, Chapter 9; Franzen 1987; Ruckhard Nicas															

Reference list for survey of analyzed ciliated ducts (in alphabetic order)

Apfeld, J. and Kenyon, C. (1999) 'Regulation of lifespan by sensory perception in Caenorhabditis elegans', *Nature*, 402(6763), p. 804. Available at: https://doi.org/10.1038/45544.

Asadzadeh, S.S. *et al.* (2019) 'Hydrodynamics of the leucon sponge pump', *Journal of The Royal Society Interface*, 16(150), p. 20180630. Available at: https://doi.org/10.1098/rsif.2018.0630.

Baeumler, N., Haszprunar, G. and Ruthensteiner, B. (2011) 'Development of the excretory system in the polyplacophoran mollusc, Lepidochitona corrugata: the protonephridium', *Journal of Morphology*, 272(8), pp. 972–986. Available at: https://doi.org/10.1002/jmor.10964.

Baeumler, N., Haszprunar, G. and Ruthensteiner, B. (2012) 'Development of the excretory system in a polyplacophoran mollusc: stages in metanephridial system development', *Frontiers in Zoology*, 9(1), p. 23. Available at: https://doi.org/10.1186/1742-9994-9-23.

Bartolomaeus, T. (1985) 'Ultrastructure and Development of the Protonephridia of Lineus viridis (Nemertini)', *Microfauna Marina*, 2, pp. 61–83.

Bartolomaeus, T. (1989) 'Ultrastructure and development of the nephridia in Anaitides mucosa (Annelida, Polychaeta)', *Zoomorphology*, 109(1), pp. 15–32. Available at: https://doi.org/10.1007/BF00312180.

Bartolomaeus, T., Maslakova, S. and von Döhren, J. (2014) 'Protonephridia in the larvae of the paleonemertean species Carinoma mutabilis (Carinomidae, Nemertea) and Cephalothrix (Procephalothrix) filiformis (Cephalothricidae, Nemertea)', *Zoomorphology*, 133(1), pp. 43–57. Available at: https://doi.org/10.1007/s00435-013-0206-3.

Biuw, L.W. and Hulting, G. (1971) 'Fine-grained secretory cells in the intestine of the lancelet, Branchiostoma (Amphioxus) lanceolatum, studied by light microscopy', *Zeitschrift für Zellforschung und Mikroskopische Anatomie*, 120(4), pp. 546–554. Available at: https://doi.org/10.1007/BF00340588.

Bolton, P.M. and Beuchat, C.A. (1991) 'Cilia in the Urinary Bladder of Reptiles and Amphibians: A Correlate of Urate Production?', *Copeia*, 1991(3), p. 711. Available at: https://doi.org/10.2307/1446397.

Bonifacio, A. *et al.* (2012) 'Nature, Source and Function of Pigments in Tardigrades: In Vivo Raman Imaging of Carotenoids in Echiniscus blumi', *PLOS ONE*, 7(11), p. e50162. Available at: https://doi.org/10.1371/journal.pone.0050162.

Boorman, C.J. and Shimeld, S.M. (2002) 'Pitx homeobox genes in Ciona and amphioxus show left-right asymmetry is a conserved chordate character and define the ascidian adenohypophysis', *Evolution & Development*, 4(5), pp. 354–365. Available at: https://doi.org/10.1046/j.1525-142x.2002.02021.x.

Brandenburg, J. and Kümmel, G. (1961) 'Die feinstruktur der solenocyten', *Journal of Ultrastructure Research*, 5(5), pp. 437–452. Available at: https://doi.org/10.1016/S0022-5320(61)80018-X.

Bresciani, J. and Fenchel, T. (1967) 'Studies on dicyemid mesozoa II. The fine structure of the infusoriform larva', *Ophelia*, 4(1), pp. 1–18. Available at: https://doi.org/10.1080/00785326.1967.10409609.

Brockmann, C. *et al.* (2001) 'The female genital system of Ooperipatellus decoratus (Onychophora, Peripatopsidae): an ultrastructural study', *Journal of Morphology*, 249(2), pp. 77–88. Available at: https://doi.org/10.1002/jmor.1041.

Brusca, R.C., Moore, W. and Shuster, S.M. (2016) *Invertebrates*. 3 edition. Sunderland, Massachusetts U.S.A: Sinauer Associates is an imprint of Oxford University Press.

Buchsbaum, R. *et al.* (2013) *Animals Without Backbones: An Introduction to the Invertebrates*. University of Chicago Press.

Buckland-Nicks, J., Lundin, K. and Wallberg, A. (2019) 'The sperm of Xenacoelomorpha revisited: implications for the evolution of early bilaterians', *Zoomorphology*, 138(1), pp. 13–27. Available at: https://doi.org/10.1007/s00435-018-0425-8.

Bunke, D. (1994) 'Ultrastructure of the metanephridial system in Aeolosoma bengalense (Annelida)', *Zoomorphology*, 114(4), pp. 247–258. Available at: https://doi.org/10.1007/BF00416863.

Burighel, P. *et al.* (2001) 'Gut Ultrastructure of the Appendicularian Oikopleura dioica (Tunicata)', *Invertebrate Biology*, 120(3), pp. 278–293.

Bustamante-Marin, X.M. and Ostrowski, L.E. (2017) 'Cilia and Mucociliary Clearance', *Cold Spring Harbor Perspectives in Biology*, 9(4). Available at: https://doi.org/10.1101/cshperspect.a028241.

Curach, N. and Sunnucks, P. (1999) 'Molecular anatomy of an onychophoran: compartmentalized sperm storage and heterogeneous paternity', *Molecular Ecology*, 8(9), pp. 1375–1385. Available at: https://doi.org/10.1046/j.1365-294x.1999.00698.x.

Delaval, B. *et al.* (2011) 'Centrin depletion causes cyst formation and other ciliopathy-related phenotypes in zebrafish', *Cell Cycle*, 10(22), pp. 3964–3972. Available at: https://doi.org/10.4161/cc.10.22.18150.

Dempsey, L.C. and Nielsen, S.L. (1976) 'Surface ultrastructure of human ependyma', *Journal of Neurosurgery*, 45(1), pp. 52–55. Available at: https://doi.org/10.3171/jns.1976.45.1.0052.

Deyts, C. *et al.* (2006) 'Morphological and gene expression similarities suggest that the ascidian neural gland may be osmoregulatory and homologous to vertebrate peri-ventricular organs', *The European Journal of Neuroscience*, 24(8), pp. 2299–2308. Available at: https://doi.org/10.1111/j.1460-9568.2006.05073.x.

Dunn, C.W., Leys, S.P. and Haddock, S.H.D. (2015) 'The hidden biology of sponges and ctenophores', *Trends in Ecology & Evolution*, 30(5), pp. 282–291. Available at: https://doi.org/10.1016/j.tree.2015.03.003.

Essock-Burns, T. *et al.* (2020) 'Interactions of Symbiotic Partners Drive the Development of a Complex Biogeography in the Squid-Vibrio Symbiosis', *mBio*, 11(3). Available at: https://doi.org/10.1128/mBio.00853-20.

Faubel, R. *et al.* (2016) 'Cilia-based flow network in the brain ventricles', *Science (New York, N.Y.)*, 353(6295), pp. 176–178. Available at: https://doi.org/10.1126/science.aae0450.

Ferguson, J.C. (1996) 'Madreporite Function and Fluid Volume Relationships in Sea Urchins', *Biological Bulletin*, 191(3), pp. 431–440. Available at: https://doi.org/10.2307/1543016.

Flores-Delgado, G., Lytle, C. and Quinton, P.M. (2015) 'Site of Fluid Secretion in Small Airways', *American Journal of Respiratory Cell and Molecular Biology*, 54(3), pp. 312–318. Available at: https://doi.org/10.1165/rcmb.2015-0238RC.

Fontaneto, D. *et al.* (2015) *Gastrotricha and Gnathifera*. Available at: https://doi.org/10.1515/9783110274271.

Forchielli, A. *et al.* (2012) 'Taphonomy of the Earliest Cambrian Linguliform Brachiopods', *Acta Palaeontologica Polonica*, 59(1), pp. 185–207. Available at: https://doi.org/10.4202/app.2011.0182.

Franzén, Å. and Afzelius, B.A. (1987) 'The ciliated epidermis of Xenoturbella bocki (Platyhelminthes, Xenoturbellida) with some phylogenetic considerations', *Zoologica Scripta*, 16(1), pp. 9–17. Available at: https://doi.org/10.1111/j.1463-6409.1987.tb00046.x.

Furuya, H. (1999) 'Fourteen New Species of Dicyemid Mesozoans from Six Japanese Cephalopods, with Comments on Host Specificity', *Species Diversity*, 4(2), pp. 257–319. Available at: https://doi.org/10.12782/specdiv.4.257.

Furuya, H., Tsuneki, K. and Koshida, Y. (1997) 'Fine structure of dicyemid mesozoans, with special reference to cell junctions', p. 9.

Gemmill, J.F. (1918) 'Ciliary Action in the Internal Cavities of the Ctenophore Pleurobrachia pileus Fabr', *Proceedings of the Zoological Society of London*, 88(3–4), pp. 263–265. Available at: https://doi.org/10.1111/j.1096-3642.1918.tb02097.x.

Gerdol, M. *et al.* (2018) 'Genetic and molecular basis of the immune system in the brachiopod Lingula anatina', *Developmental & Comparative Immunology*, 82, pp. 7–30. Available at: https://doi.org/10.1016/j.dci.2017.12.021.

Gruhl, A., Wegener, I. and Bartolomaeus, T. (2009) 'Ultrastructure of the body cavities in Phylactolaemata (Bryozoa)', *Journal of Morphology*, 270(3), pp. 306–318. Available at: https://doi.org/10.1002/jmor.10691.

Han, J. and Sadiq, N.M. (2020) 'Anatomy, Abdomen and Pelvis, Fallopian Tube', in *StatPearls*. Treasure Island (FL): StatPearls Publishing. Available at: http://www.ncbi.nlm.nih.gov/books/NBK547660/ (Accessed: 12 March 2020).

Hanelt, B., Thomas, F. and Schmidt-Rhaesa, A. (2005) 'Biology of the Phylum Nematomorpha', in J.R. Baker, R. Muller, and D. Rollinson (eds) *Advances in Parasitology*. Academic Press, pp. 243–305. Available at: https://doi.org/10.1016/S0065-308X(05)59004-3.

Harmata, K.L. *et al.* (2013) 'Quantitative measures of gastrovascular flow in octocorals and hydroids: toward a comparative biology of transport systems in cnidarians', *Invertebrate Biology*, 132(4), pp. 291–304. Available at: https://doi.org/10.1111/ivb.12028.

Hay-Schmidt, A. (1987) 'The Ultrastructure of the Protonephridium of the Actinotroch Larva (Phoronida)', *Acta Zoologica*, 68(1), pp. 35–47. Available at: https://doi.org/10.1111/j.1463-6395.1987.tb00874.x.

He, C. *et al.* (2018) 'Phagocytic intracellular digestion in amphioxus (Branchiostoma)', *Proceedings of the Royal Society B: Biological Sciences*, 285(1880), p. 20180438. Available at: https://doi.org/10.1098/rspb.2018.0438.

Hess, R.A. (2015) 'Small tubules, surprising discoveries: from efferent ductules in the turkey to the discovery that estrogen receptor alpha is essential for fertility in the male', *Animal reproduction*, 12(1), pp. 7–23.

Holmberg, K. (1982) 'The Ciliated Brain Duct of Oikopleura dioica (Tunicata, Appendicularia)', *Acta Zoologica*, 63(2), pp. 101–109. Available at: https://doi.org/10.1111/j.1463-6395.1982.tb00765.x.

Hopcroft, R.R. and Robison, B.H. (2005) 'New mesopelagic larvaceans in the genus Fritillaria from Monterey Bay, California', *Journal of the Marine Biological Association of the United Kingdom*, 85(3), pp. 665–678. Available at: https://doi.org/10.1017/S0025315405011598.

Jiménez, A.J. *et al.* (2014) 'Structure and function of the ependymal barrier and diseases associated with ependyma disruption', *Tissue Barriers*, 2(1), p. e28426. Available at: https://doi.org/10.4161/tisb.28426.

Kato, C., Lehrke, J. and Quast, B. (2011) 'Ultrastructure and phylogenetic significance of the head kidneys in Thalassema thalassemum (Thalassematinae, Echiura)', *Zoomorphology*, 130(2), pp. 97–106. Available at: https://doi.org/10.1007/s00435-011-0124-1.

Kieneke, A. *et al.* (2008) 'Ultrastructure of protonephridia in Xenotrichula carolinensis syltensis and Chaetonotus maximus (Gastrotricha: Chaetonotida): comparative evaluation of the gastrotrich excretory organs', *Zoomorphology*, 127(1), pp. 1–20. Available at: https://doi.org/10.1007/s00435-007-0051-3.

Kristensen, R.M. and Funch, P. (2000) 'Micrognathozoa: a new class with complicated jaws like those of Rotifera and Gnathostomulida', *Journal of Morphology*, 246(1), pp. 1–49. Available at: https://doi.org/10.1002/1097-4687(200010)246:1<1::AID-JMOR1>3.0.CO;2-D.

Kümmel, G. (1962) 'Zwei neue Formen von Cyrtocyten. Vergleich der bisher bekannten Cyrtocyten und Erörterung des Begriffes „Zelltyp"', *Zeitschrift für Zellforschung und Mikroskopische Anatomie*, 57(2), pp. 172–201. Available at: https://doi.org/10.1007/BF00319392.

Lambot, M.-A.H. *et al.* (2009) 'Three-Dimensional Reconstruction of Efferent Ducts in Wild-Type and *Lgr4* Knock-Out Mice', *The Anatomical Record: Advances in Integrative Anatomy and Evolutionary Biology*, 292(4), pp. 595–603. Available at: https://doi.org/10.1002/ar.20883.

Lammert, V. (1985) 'The fine structure of protonephridia in Gnathostomulida and their comparison within Bilateria', *Zoomorphology*, 105(5), pp. 308–316. Available at: https://doi.org/10.1007/BF00312062.

Lee, K.H. *et al.* (2000) 'Estrogen receptor alpha has a functional role in the mouse rete testis and efferent ductules', *Biology of Reproduction*, 63(6), pp. 1873–1880.

Lee, M.-S. *et al.* (2015) 'IFT46 plays an essential role in cilia development', *Developmental Biology*, 400(2), pp. 248–257. Available at: https://doi.org/10.1016/j.ydbio.2015.02.009.

Leys, S.P. *et al.* (2011) 'The Sponge Pump: The Role of Current Induced Flow in the Design of the Sponge Body Plan', *PLOS ONE*, 6(12), p. e27787. Available at: https://doi.org/10.1371/journal.pone.0027787.

Leys, S.P. and Eerkes-Medrano, D.I. (2006) 'Feeding in a calcareous sponge: particle uptake by pseudopodia', *The Biological Bulletin*, 211(2), pp. 157–171. Available at: https://doi.org/10.2307/4134590.

López-Urrutia, Á. and Acuña, J.L. (1999) 'Gut throughput dynamics in the appendicularian Oikopleura dioica', *Marine Ecology Progress Series*, 191, pp. 195–205.

Ma, W. *et al.* (2022) 'Alleviation of Tris(2-chloroethyl) Phosphate Toxicity on the Marine Rotifer Brachionus plicatilis by Polystyrene Microplastics: Features and Molecular Evidence', *International Journal of Molecular Sciences*, 23(9), p. 4934. Available at: https://doi.org/10.3390/ijms23094934.

Manni, L. *et al.* (2005) 'Stomodeal and neurohypophysial placodes in Ciona Intestinalis: insights into the origin of the pituitary gland', *Journal of Experimental Zoology Part B: Molecular and Developmental Evolution*, 304B(4), pp. 324–339. Available at: https://doi.org/10.1002/jez.b.21039.

Matsubara, J.A. and Dudley, P.L. (1976) 'Fine Structural Studies of the Dicyemid Mesozoan, Dicyemmenea californica McConnaughey. II. The Young Vermiform Stage and the Infusoriform Larva', *The Journal of Parasitology*, 62(3), p. 390. Available at: https://doi.org/10.2307/3279147.

Mayer, G. (2006) 'Origin and differentiation of nephridia in the Onychophora provide no support for the Articulata', *Zoomorphology*, 125(1), pp. 1–12. Available at: https://doi.org/10.1007/s00435-005-0006-5.

Mayer, G. and Whitington, P.M. (2009) 'Neural development in Onychophora (velvet worms) suggests a step-wise evolution of segmentation in the nervous system of Panarthropoda', *Developmental Biology*, 335(1), pp. 263–275. Available at: https://doi.org/10.1016/j.ydbio.2009.08.011.

McKanna, J.A. (1968) 'Fine structure of the protonephridial system in planaria, II. Ductules, Collecting Ducts, and Osmoregulatory Cells', *Zeitschrift ftir Zellforschung*, 92, pp. 524–535.

Meyrick, B., Sturgess, J.M. and Reid, L. (1969) 'A reconstruction of the duct system and secretory tubules of the human bronchial submucosal gland', *Thorax*, 24(6), pp. 729–736. Available at: https://doi.org/10.1136/thx.24.6.729.

Møbjerg, N., Jespersen, Å. and Wilkinson, M. (2004) 'Morphology of the kidney in the West African caecilian, *Geotrypetes seraphini* (Amphibia, Gymnophiona, Caeciliidae): Kidney Morphology in *G. seraphini*', *Journal of Morphology*, 262(2), pp. 583–607. Available at: https://doi.org/10.1002/jmor.10244.

Møbjerg, N., Larsen, E.H. and Jespersen, Å. (1998) 'Morphology of the Nephron in the Mesonephros of *Bufo bufo* (Amphibia, Anura, Bufonidae)', *Acta Zoologica*, 79(1), pp. 31–50. Available at: https://doi.org/10.1111/j.1463-6395.1998.tb01140.x.

Møbjerg, N., Larsen, E.H. and Jespersen, A. (2000) 'Morphology of the kidney in larvae of Bufo viridis (Amphibia, Anura, Bufonidae)', *Journal of Morphology*, 245(3), pp. 177–195. Available at: https://doi.org/10.1002/1097-4687(200009)245:3<177::AID-JMOR1>3.0.CO;2-F.

Moller, P.C. and Ellis, R.A. (1974) 'Fine structure of the excretory system of Amphioxus (Branchiostoma floridae) and its response to osmotic stress', *Cell and Tissue Research*, 148(1), pp. 1–9. Available at: https://doi.org/10.1007/BF00224314.

Morris, JudithL. (1981) 'Structure and function of ciliated peritoneal funnels in the toad kidney (Bufo marinus)', *Cell and Tissue Research*, 217(3), pp. 599–610. Available at: https://doi.org/10.1007/BF00219367.

Neuhaus, B. (1988) 'Ultrastructure of the protonephridia in Pycnophyes kielensis (Kinorhyncha, Homalorhagida)', *Zoomorphology*, 108(4), pp. 245–253. Available at: https://doi.org/10.1007/BF00312224.

Neuhaus, B. and Kristensen, R.M. (2007) 'Ultrastructure of the protonephridia of larval *Rugiloricus* cf. *cauliculus* , male *Armorloricus elegans* , and female *Nanaloricus mysticus* (Loricifera)', *Journal of Morphology*, 268(4), pp. 357–370. Available at: https://doi.org/10.1002/jmor.10521.

Neves, R.C. *et al.* (2010) 'Comparative myoanatomy of cycliophoran life cycle stages', *Journal of Morphology*, 271(5), pp. 596–611. Available at: https://doi.org/10.1002/jmor.10819.

Norekian, T.P. and Moroz, L.L. (2019) 'Neural system and receptor diversity in the ctenophore Beroe abyssicola', *The Journal of Comparative Neurology*, 527(12), pp. 1986–2008. Available at: https://doi.org/10.1002/cne.24633.

Ott, E. *et al.* (2016) 'Pronephric tubule morphogenesis in zebrafish depends on Mnx mediated repression of irx1b within the intermediate mesoderm', *Developmental Biology*, 411(1), pp. 101–114. Available at: https://doi.org/10.1016/j.ydbio.2015.10.014.

Perez, Y., Casanova, J.-P. and Mazza, J. (2000) 'Changes in the structure and ultrastructure of the intestine of Spadella cephaloptera (Chaetognatha) during feeding and starvation experiments', *Journal of Experimental Marine Biology and Ecology*, 253(1), pp. 1–15. Available at: https://doi.org/10.1016/S0022-0981(00)00228-8.

Perez, Y., Casanova, J.-P. and Mazza, J. (2001) 'Degrees of vacuolation of the absorptive intestinal cells of five Sagitta (Chaetognatha) species: possible ecophysiological implications', *Marine Biology*, 138(1), pp. 125–133. Available at: https://doi.org/10.1007/s002270000438.

Presnell, J.S. *et al.* (2016) 'The Presence of a Functionally Tripartite Through-Gut in Ctenophora Has Implications for Metazoan Character Trait Evolution', *Current Biology*, 26(20), pp. 2814–2820. Available at: https://doi.org/10.1016/j.cub.2016.08.019.

Purschke, G. and Tzetlin, A.B. (1996) 'Dorsolateral Ciliary Folds in the Polychaete Foregut: Structure, Prevalence and Phylogenetic Significance', *Acta Zoologica*, 77(1), pp. 33–49. Available at: https://doi.org/10.1111/j.1463-6395.1996.tb01251.x.

Raidt, J. *et al.* (2015) 'Ciliary function and motor protein composition of human fallopian tubes', *Human Reproduction (Oxford, England)*, 30(12), pp. 2871–2880. Available at: https://doi.org/10.1093/humrep/dev227.

Reiten, I. *et al.* (2017) 'Motile-Cilia-Mediated Flow Improves Sensitivity and Temporal Resolution of Olfactory Computations', *Current Biology*, 27(2), pp. 166–174. Available at: https://doi.org/10.1016/j.cub.2016.11.036.

Rheubert, J.L., Siegel, D.S. and Trauth, S.E. (2014) *Reproductive Biology and Phylogeny of Lizards and Tuatara*. CRC Press.

Riisgård, H.U., Funch, P. and Larsen, P.S. (2015) 'The mussel filter–pump – present understanding, with a re-examination of gill preparations', *Acta Zoologica*, 96(3), pp. 273–282. Available at: https://doi.org/10.1111/azo.12110.

Riisgård, H.U., Larsen, P.S. and Nielsen, N.F. (1996) 'Particle capture in the musselMytilus edulis: The role of latero-frontal cirri', *Marine Biology*, 127(2), pp. 259–266. Available at: https://doi.org/10.1007/BF00942111.

Rink, J.C., Vu, H.T.-K. and Sánchez Alvarado, A. (2011) 'The maintenance and regeneration of the planarian excretory system are regulated by EGFR signaling', *Development (Cambridge, England)*, 138(17), pp. 3769–3780. Available at: https://doi.org/10.1242/dev.066852.

Rohde, K. and Watson, N.A. (1992) 'Ultrastructure of the Flame Bulbs and Protonephridial Capillaries of *Artioposthia* sp. (Platyhelminthes, Tricladida, Geoplanidae)', *Acta Zoologica*, 73(4), pp. 231–236. Available at: https://doi.org/10.1111/j.1463-6395.1992.tb01087.x.

Ruppert, E.E. (1990) 'Structure, Ultrastructure and Function of the Neural Gland Complex of *Ascidia interrupta* (Chordata, Ascidiacea): Clarification of Hypotheses Regarding the Evolution of the Vertebrate Anterior Pituitary', *Acta Zoologica*, 71(3), pp. 135–149. Available at: https://doi.org/10.1111/j.1463-6395.1990.tb01189.x.

Ruppert, E.E. (1996) 'Morphology of Hatschek's nephridium in larval and juvenile stages of Branchiostoma virginiae (Cephalochordata)', 42, pp. 161–182.

Schramm, U. (1978) 'On the excretory system of the rotifer Habrotrocha rosa donner', *Cell and Tissue Research*, 189(3). Available at: https://doi.org/10.1007/BF00209137.

Schwaha, T., Wood, T.S. and Wanninger, A. (2010) 'Trapped in freshwater: the internal anatomy of the entoproct Loxosomatoides sirindhornae', *Frontiers in Zoology*, 7, p. 7. Available at: https://doi.org/10.1186/1742-9994-7-7.

Sharaf, A., Eid, W. and Abuel-Atta, A.A. (2013) 'Age-related morphology of the ostrich oviduct (isthmus, uterus and vagina)', *Bulgarian Journal of Veterinary Medicine*, 16(3), p. 15.

Sherlock, R.E. *et al.* (2016) 'Morphology, ecology, and molecular biology of a new species of giant larvacean in the eastern North Pacific: Bathochordaeus mcnutti sp. nov.', *Marine Biology*, 164(1), p. 20. Available at: https://doi.org/10.1007/s00227-016-3046-0.

Sherlock, R.E., Walz, K.R. and Robison, B.H. (2016) 'The first definitive record of the giant larvacean, Bathochordaeus charon, since its original description in 1900 and a range extension to the northeast Pacific Ocean', *Marine Biodiversity Records*, 9(1), p. 79. Available at: https://doi.org/10.1186/s41200-016-0075-9.

Smith, C.L., Pivovarova, N. and Reese, T.S. (2015) 'Coordinated Feeding Behavior in Trichoplax, an Animal without Synapses', *PLoS ONE*, 10(9). Available at: https://doi.org/10.1371/journal.pone.0136098.

Storch, V., Higgins, R.P. and Morse, M.P. (1989) 'Internal Anatomy of Meiopriapulus fijiensis (Priapulida)', *Transactions of the American Microscopical Society*, 108(3), pp. 245–261. Available at: https://doi.org/10.2307/3226343.

Storch, V.V., Ruhberg, H. and Alberti, G. (1978) 'Zur Ultrastruktur der Segmentalorgane der Peripatopsidae (Onychophora)', *Zool. Jb. Anat. Bd.*, 100, pp. 47–63.

Suzuki, A.C. and Kristensen, R.M. (2014) 'Spermatozoa in the reproductive system of a hermaphroditic marine tardigrade, Orzeliscus belopus (Tardigrada: Arthrotardigrada)', *Zoologischer Anzeiger - A Journal of Comparative Zoology*, 253(6), pp. 497–511. Available at: https://doi.org/10.1016/j.jcz.2014.07.003.

Tamm, S.L. (2014) 'Cilia and the life of ctenophores', *Invertebrate Biology*, 133(1), pp. 1–46. Available at: https://doi.org/10.1111/ivb.12042.

Tamori, M., Matsuno, A. and Takahashi, K. (1996) 'Structure and Function of the Pore Canals of the Sea Urchin Madreporite', *Philosophical Transactions: Biological Sciences*, 351(1340), pp. 659–676.

Temereva, E.N. (2010) 'The digestive tract of actinotroch larvae (Lophotrochozoa, Phoronida): anatomy, ultrastructure, innervations, and some observations of metamorphosis', *Canadian Journal of Zoology*, 88(12), pp. 1149–1168. Available at: https://doi.org/10.1139/Z10-075.

Valverde-Islas, L.E. *et al.* (2011) 'Visualization and 3D Reconstruction of Flame Cells of Taenia solium (Cestoda)', *PLoS ONE*, 6(3). Available at: https://doi.org/10.1371/journal.pone.0014754.

Vasilyev, A. *et al.* (2012) 'Mechanical Stretch and PI3K Signaling Link Cell Migration and Proliferation to Coordinate Epithelial Tubule Morphogenesis in the Zebrafish Pronephros', *PLoS ONE*. Edited by F. Pichaud, 7(7), p. e39992. Available at: https://doi.org/10.1371/journal.pone.0039992.

Warner, F.D. (1969) 'The Fine Structure of the Protonephridio in the Rotifer Asplanchna', *J Ultrastructure Research*, 29, pp. 499–524.

Weibel, E.R. (1963) *Morphometry of the Human Lung*. Berlin Heidelberg: Springer-Verlag. Available at: https://doi.org/10.1007/978-3-642-87553-3.

Westbroek, P. (1968) 'Morphological observations with systematic implications on some palaeozoic Rhynchonellida from Europe, with special emphasis on the Uncinulidae', *Leidse Geologische Mededelingen*, 41(1), pp. 1–82.

Westbroek, P., Yanagida, J. and Isa, Y. (1980) 'Functional Morphology of Brachiopod and Coral Skeletal Structures Supporting Ciliated Epithelia', *Paleobiology*, 6(3), pp. 313–330.

Worsaae, K. *et al.* (2012) 'An Anatomical Description of a Miniaturized Acorn Worm (Hemichordata, Enteropneusta) with Asexual Reproduction by Paratomy', *PLoS ONE*. Edited by A. Hejnol, 7(11), p. e48529. Available at: https://doi.org/10.1371/journal.pone.0048529.

Worthington, W.C. and Cathcart, R.S. (1963) 'Ependymal cilia: distribution and activity in the adult human brain', *Science (New York, N.Y.)*, 139(3551), pp. 221–222. Available at: https://doi.org/10.1126/science.139.3551.221.

Xiong, G. *et al.* (2014) 'Traumatic Brain Injury-Induced Ependymal Ciliary Loss Decreases Cerebral Spinal Fluid Flow', *Journal of Neurotrauma*, 31(16), pp. 1396–1404. Available at: https://doi.org/10.1089/neu.2013.3110.

Yu, J.-P. and Cui, S.-J. (1997) 'Ultrastructure of the rotifer Brachionus plicatilis', in A. Hagiwara et al. (eds) *Live Food in Aquaculture*. Dordrecht: Springer Netherlands (Developments in Hydrobiology), pp. 95–103. Available at: https://doi.org/10.1007/978-94-017-2097-7_15.

Yuan, S. *et al.* (2019) 'Motile cilia of the male reproductive system require miR-34/miR-449 for development and function to generate luminal turbulence', *Proceedings of the National Academy of Sciences*, 116(9), pp. 3584–3593. Available at: https://doi.org/10.1073/pnas.1817018116.

Zhang, Q. *et al.* (2012) 'Knockdown of *ttc26* disrupts ciliogenesis of the photoreceptor cells and the pronephros in zebrafish', *Molecular Biology of the Cell*. Edited by E. Holzbaur, 23(16), pp. 3069–3078. Available at: https://doi.org/10.1091/mbc.e12-01-0019.

Zhuravlova, I., Kornieieva, M. and Rodrigues, E. (2018) 'Anatomic Variability of the Morphometric Parameters of the Fourth Ventricle of the Brain', *Journal of Neurological Surgery. Part B, Skull Base*, 79(2), pp. 200–204. Available at: https://doi.org/10.1055/s-0037-1606331.

Zverkov, O.A. *et al.* (2019) 'Dicyemida and Orthonectida: Two Stories of Body Plan Simplification', *Frontiers in Genetics*, 10. Available at: https://doi.org/10.3389/fgene.2019.00443.